Two-Photon Absorption for Optical Clock Recovery in OTDM Networks

Reza Salem, *Student Member, IEEE*, Amir Ali Ahmadi, Gaston E. Tudury, Gary M. Carter, *Senior Member, IEEE*, and Thomas E. Murphy, *Member, IEEE*

***Abstract*—The authors describe the design and performance of an ultrafast optical clock recovery system that is based on two-photon absorption (TPA) in a silicon avalanche photodiode. Unlike many other optical clock recovery techniques, the system is shown to be polarization insensitive, broadband, low jitter, and scalable to high data rates. Moreover, the system is simple, economical, and suitable for integration with silicon electronics. Successful operation of the system is reported for speeds up to 80 Gb/s and transmission distances up to 840 km using a recirculating loop. The authors introduce a new dithering detection scheme that dramatically improves the dynamic range and decreases polarization and wavelength dependence, without introducing an additional timing jitter. The system achieves a dynamic range of 10 dB and optical bandwidth exceeding 35 nm.**

***Index Terms*—Nonlinear optics, optical communication, optical-signal processing, phase-locked loops (PLLs), photodiodes, polarization, synchronization, timing jitter.**

I. Introduction

CLOCK recovery, which is the process of synchronizing a locally generated clock with incoming data, is a prerequisite for most other optical processing tasks including optical demultiplexing, optical logic, and optical retiming, recompression, and reamplification (3R) regeneration. Although electronic circuits can perform clock recovery at speeds up to 40 Gb/s, in future optical time-division multiplexed networks, the data rate could exceed the speed of conventional electronics. In these systems, the process of clock recovery can be better accomplished in the optical domain.

Techniques previously used for optical clock recovery include injection-locked laser cavities [1]–[3], electrical ring oscillators [4]–[6], and a variety of optical phase-locked loop (PLL) systems [7]–[12]. Among the PLL methods, many nonlinear processes have been employed for timing detection, including four-wave mixing in fiber [7] or semiconductor waveguides [8], cross-absorption modulation in an electroabsorption modulator (EAM) [9], cross-phase-modulation in semiconductor amplifiers [10], and optoelectronic mixing in modulators [11], [13]. Although these methods have enabled subharmonic clock recovery at speeds up to hundreds of gigabits per second, few of these techniques provide polarization and wavelength independence comparable to what is routinely achieved in slower electronic clock recovery systems.

Methods for mitigating the polarization dependence include polarization interleaving [14], in which neighboring pulses are orthogonally polarized, and polarization diversity [15], [16], in which the optical signal is split into orthogonally polarized components that are processed separately. Each of these techniques introduces an additional complexity in the system that would not be necessary if the underlying optical process were itself polarization independent. Injection-locking techniques have been shown to have a lower polarization dependence [1], but they are usually tied to a specific repetition frequency and wavelength.

Wavelength dependence is another challenge associated with the optical clock recovery. With the exception of DFB lasers, most components in optical communication systems (e.g., modulators, amplifiers, and photodetectors) can be used for many different wavelength channels without incurring a significant penalty. By contrast, many of the nonlinear optical techniques used in optical clock recovery systems require specific wavelengths for both the clock and data. In some cases, the clock and data must be sufficiently separated in wavelength to be spectrally distinguishable, as, for example, when an optical filter is used to separate the clock and data after mixing. In some cases, the clock and the data cannot be too far apart because the nonlinear mixing efficiency decreases with separation. For many nonlinear processes, the attainable wavelength range is limited by phase-matching conditions or the wavelength characteristics of the devices used. In wavelength-division multiplexed networks, it is especially important that the clock recovery not be constrained in wavelength.

In this paper, we describe a new clock recovery system that is based on two-photon absorption (TPA) in a silicon photodiode. Unlike many other nonlinear processes, TPA is simple, inexpensive, and ultrafast. More significantly, we will demonstrate that the system shows very little polarization dependence and broad wavelength range—overcoming two critical problems that have historically plagued the optical clock recovery systems. We will derive analytical expressions for the cross-correlation signal, which is generated by TPA in terms of the input powers and polarization states. Using these theoretical guidelines, we design a PLL with a low polarization dependence. We demonstrate the operation of this system in

Manuscript received December 7, 2005; revised June 4, 2006. This work was supported in part by the National Science Foundation (NSF) under CAREER Grant 0546928.

R. Salem, A. A. Ahmadi, and T. E. Murphy are with the Department of Electrical and Computer Engineering, University of Maryland, College Park, MD 20742 USA (e-mail: rsalem@eng.umd.edu; amalahmadi@yahoo.com; tem@umd.edu).

G. E. Tudury is with the Laboratory for Physical Sciences, College Park, MD 20740 USA (e-mail: getudury@gmail.com).

G. M. Carter is with the Department of Computer Science and Electrical Engineering, University of Maryland Baltimore County, Baltimore, MD 21250 USA (e-mail: carter@umbc.edu).

Digital Object Identifier 10.1109/JLT.2006.880159

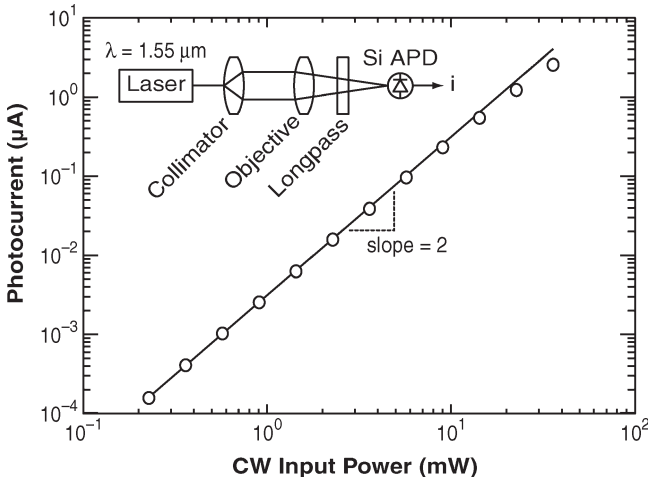

Fig. 1. Measured photocurrent as a function of the CW optical input power for the silicon avalanche photodiode used in this paper.

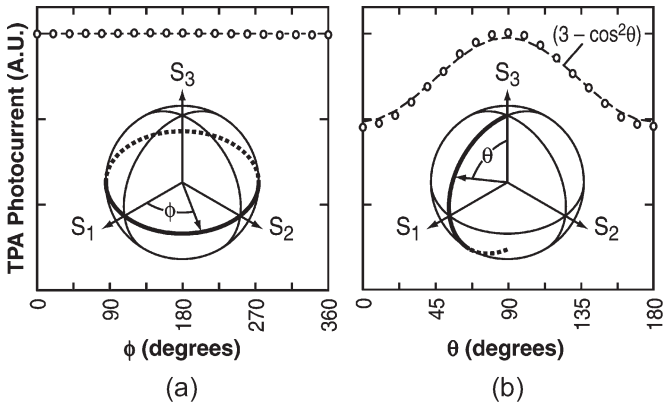

Fig. 2. Measured photocurrent produced by TPA as a function of the polarization state. (a) Photocurrent produced by TPA is the same for all linear polarization states. (b) When the polarization state changes from linear to circular, the photocurrent decreases by a factor of approximately 2/3.

an 80-Gb/s transmission system, achieving error-free operation after an 840-km transmission without polarization control. Finally, we introduce a new optical dithering system that improves the dynamic range and further reduces the polarization sensitivity without introducing additional timing jitter in the recovered clock.

II. Optical Cross Correlation Using TPA

One key ingredient in the PLL clock recovery system is a phase detector: a device that measures the relative timing between the clock and the data. In electrical clock recovery systems, the phase detection is accomplished by mixing the photodetected data and the electrical clock in a microwave mixer. In the optical clock recovery system reported here, the mixer is replaced with a much faster nonlinear optical process that operates directly on the optical signals.

The nonlinear process that we use is TPA: an ultrafast process in which two photons are simultaneously absorbed in a photodiode to generate a single electron-hole pair. Unlike conventional photodetection, TPA produces a photocurrent proportional to the square of the optical power. Because of this quadratic nonlinearity, TPA can be used to measure the correlation between high-speed optical signals in much the same way that a sum-frequency generation is used in optical autocorrelators to diagnose pulses that are too short to be measured electrically.

Fig. 1 plots the measured photocurrent as a function of the input optical power for the silicon avalanche photodiode used in this paper, clearly showing the quadratic relationship over several orders of magnitude. In these measurements, a continuous-wave (CW) optical signal at 1550 nm was focused through a microscope objective to a 3-μm spot on the surface of the silicon detector. A long-pass filter was inserted to block any ambient light or residual pump light from the fiber amplifiers that could otherwise produce a linear photocurrent.

Because the polarization state cannot be easily controlled in the optical fiber, it is important to understand how TPA depends on the polarization state. Fig. 2 plots the measured TPA photocurrent as a function of the input polarization state when the power is fixed. While the photocurrent is the same for all linear polarization states, it decreases by a factor of 2/3 for circular polarization states. This 2/3 circular-to-linear ratio is theoretically expected for isotropic $\chi^{(3)}$ nonlinear processes. Under the assumption that the TPA in silicon is isotropic, the photocurrent generated through TPA can be modeled by the following simple relation:

$$i_{\mathrm{TPA}} \propto \left\langle |\mathbf{E}(t)|^4 \right\rangle \tag{1}$$

where $\langle\cdot\rangle$ indicates the time-average, and $\mathbf{E}(t)$ is the real-valued electric-field vector of the light. If the optical signal is a CW signal with power P, (1) predicts that the photocurrent is given by

$$i_{\mathrm{TPA}} = \eta \left(1 - \frac{S_3^2}{3}\right) P^2 \tag{2}$$

where η is an efficiency factor for the process, and (S_1, S_2, S_3) are the normalized Stokes parameters describing the polarization state, i.e., the coordinates on the Poincaré sphere. Equation (2) predicts that for a given power P, the amount of TPA depends only on the degree of ellipticity of the polarization state, described by S_3. The dashed lines plotted in Fig. 2 were calculated using (2) and show excellent agreement with our experimental measurements.

The analysis of the polarization dependence is more complicated if there are two optical signals with different wavelengths and polarization states. For clock recovery, we are interested in the case where two optical pulses (data and clock) generate a cross-correlation signal in the detector, as shown schematically in Fig. 3(a). We assume that the difference between the optical carrier frequencies is higher than the speed of the electrical detector so that the optical beating between the clock and the data is not observed. The detector is also not fast enough to resolve the individual pulses or data patterns that make up the clock and data. Despite the limited speed of the detector, the time-averaged photocurrent depends on the relative delay (τ) between the clock and the data, as shown schematically in Fig. 3(b). The average output photocurrent $i(\tau)$ consists of the

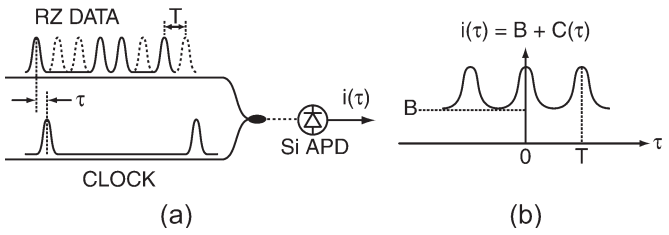

Fig. 3. Schematic of cross-correlation measurement produced by TPA. (a) Two optical signals are combined and directed to the silicon detector. (b) Time-averaged photocurrent $\langle i(\tau)\rangle$ is comprised of a cross-correlation signal $C(\tau)$ on top of a constant background level B.

intensity cross-correlation function $C(\tau)$ on top of a uniform background level B:

$$i(\tau) = B + C(\tau). \tag{3}$$

In general, both the background B and the cross correlation $C(\tau)$ depend upon the polarization states and powers in the two optical signals. When the simple model given in (1) is applied to the case of two optical signals, we find after some calculation that

$$B = \eta\left[\left\langle p^2(t)\right\rangle\left(1-\frac{S_3^2}{3}\right)+\left\langle p'^2(t)\right\rangle\left(1-\frac{S_3'^2}{3}\right)\right] \tag{4}$$

$$C(\tau) = \frac{8\eta}{3}\left\langle p(t-\tau)p'(t)\right\rangle\left(1+\frac{1}{2}S_1S_1'+\frac{1}{2}S_2S_2'\right) \tag{5}$$

where $p(t)$ and $p'(t)$ are the power envelopes of the clock signal and data, respectively, and $\mathbf{S}$ and $\mathbf{S}'$ describe their corresponding normalized Stokes vectors.

In a clock recovery system, the optical clock is generated locally, and can therefore have a prescribed polarization state, whereas the data polarization cannot be easily controlled. One important observation that follows from (5) is that by fixing the polarization of the clock signal to be circular, i.e., setting $S_1 = S_2 = 0$, the cross-correlation component becomes independent of the data polarization state. Under this condition, (4)–(5) simplify to

$$B = \eta\left[\frac{2}{3}\left\langle p^2(t)\right\rangle+\left(1-\frac{S_3^2}{3}\right)\left\langle p'^2(t)\right\rangle\right] \tag{6}$$

$$C(\tau) = \frac{8\eta}{3}\left\langle p(t-\tau)p'(t)\right\rangle. \tag{7}$$

When the clock is circularly polarized, changes in the data polarization state produce a shift in the background level, but the cross-correlation signal is unchanged. We have experimentally confirmed this prediction in an earlier work [17]. A similar effect is predicted for other third-order processes in isotropic media. For example, four-wave mixing in fiber becomes polarization independent when one of the input signals is circularly polarized [18].

III. 80 Gb/s Clock Recovery Experiment

In the optical clock recovery system, the cross correlation produced by TPA is used to measure the timing difference between the clock and the data. Fig. 4(a) depicts the cross correlation between a 10-GHz optical clock and an 80-Gb/s RZ data signal, as measured by TPA in a silicon photodiode. Although the cross-correlation function is strictly positive, a bipolar signal can be obtained by subtracting a constant offset level. The resulting bipolar signal can then be used as the error signal in a PLL to synchronize the clock and data. The PLL works to drive the error signal to zero, which locks the clock and data together with a timing difference determined by the position of the zero-crossing point, which is labeled τ_0 in the magnified view in Fig. 4(b).

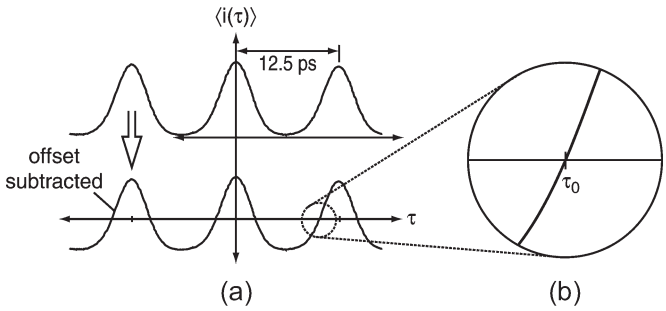

Fig. 4. (a) Measured cross correlation between 10-GHz clock and 80-Gb/s data before and after the offset is subtracted. (b) Magnified view of cross correlation, showing the zero-crossing location.

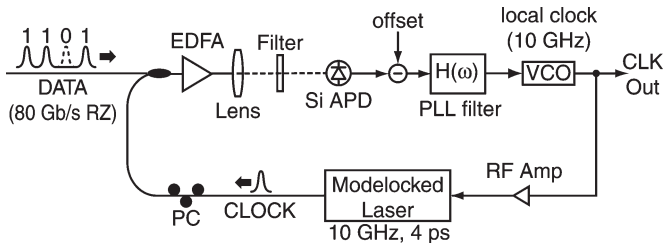

Fig. 5. Diagram of 80-Gb/s optical clock recovery system.

Fig. 5 depicts the experimental setup used to demonstrate 80-Gb/s clock recovery using TPA [19]. The 10-GHz 4-ps clock pulses were generated from a semiconductor mode-locked laser driven by an electrical voltage-controlled oscillator. Data pulses with duration of 4 ps were generated using a 10-GHz mode-locked fiber laser, which was passively multiplexed to 40 GHz and ON–OFF modulated with a $2^{23}-1$ pseudorandom binary data sequence. One additional multiplexing stage was employed to produce an 80-Gb/s data sequence. The average optical powers of data and clock signals impinging on the detector surface were 3 and 6 mW, respectively. Fig. 6 shows the optical spectrum of the combined data and clock signals. The electrical filter $H(\omega)$ was designed so that the PLL would have a closed-loop bandwidth of about 5.5 kHz.

Fig. 7 plots the electrical spectrum and single-sideband phase noise of the recovered clock in comparison to the original clock used in the transmitter. Integrating the phase-noise pedestal from 100 Hz to 10 MHz yields a timing jitter of 110 fs for the recovered clock, compared to 170 fs for the transmitter clock. In this system, the recovered clock exhibits less phase noise than the original clock, because the voltage-controlled oscillator (VCO) used in the clock recovery system is less noisy than the RF synthesizer used in the transmitter.

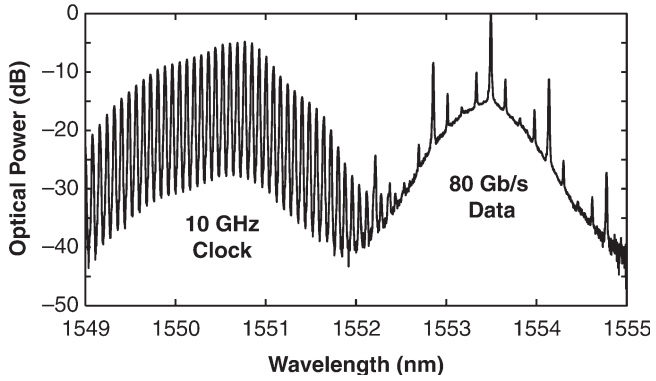

Fig. 6. Optical spectrum of the 10-GHz clock and 80-Gb/s data.

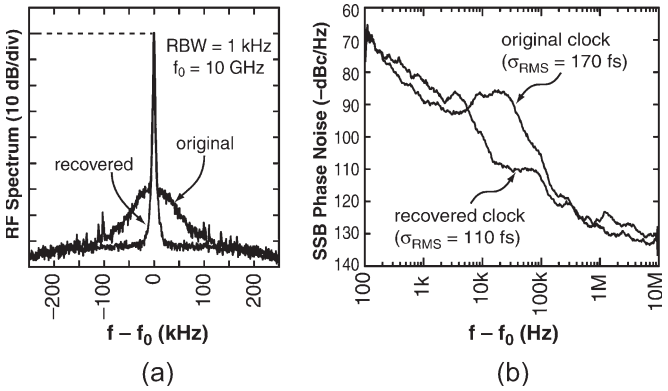

Fig. 7. (a) Measured RF spectrum and (b) single-sideband phase noise of the recovered 10-GHz electrical clock, compared to the original clock used in the transmitter.

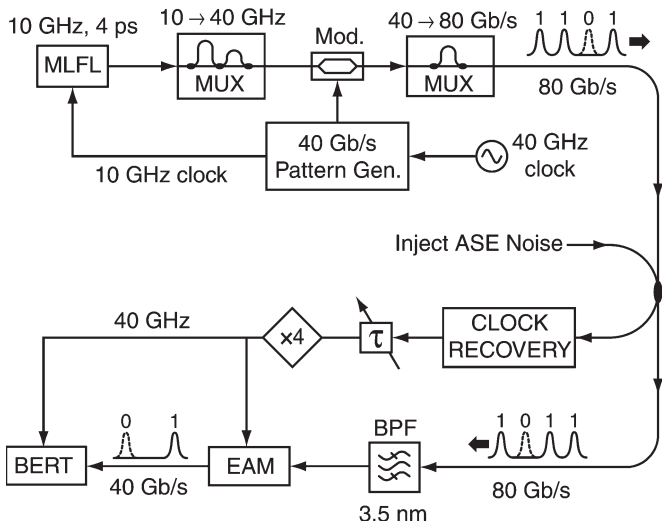

Fig. 8. Diagram of the 80-Gb/s optical transmitter, demultiplexer, and receiver used to characterize the clock recovery system. Instead of varying the received optical power, the optical OSNR was adjusted by injecting a broadband optical noise prior to the receiver.

The clock recovery system was also evaluated using bit-error-rate (BER) measurements. As depicted in Fig. 8, the data was demultiplexed from 80 to 40 Gb/s using an EAM driven by a 40-GHz signal derived from the clock recovery system. The clock recovery system requires a prescribed input power to operate, which makes it difficult to perform the conventional

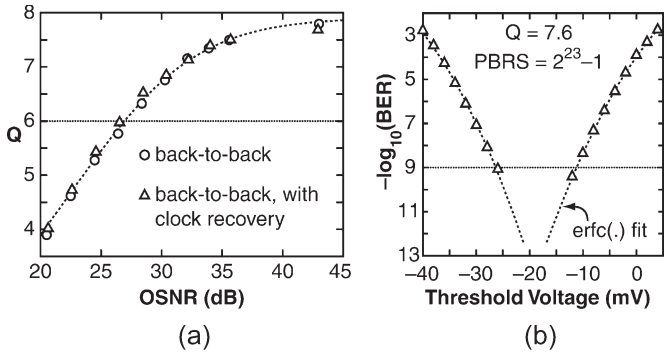

Fig. 9. (a) Measured back-to-back Q versus OSNR for the system depicted in Fig. 8 with and without the clock recovery, showing no appreciable penalty. (b) Measured BER versus decision threshold for the case when $Q = 7.6$.

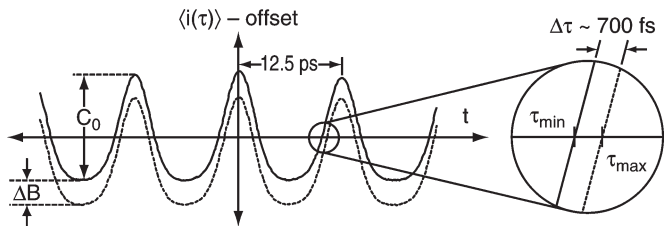

Fig. 10. Minimum and maximum cross-correlation signals obtained by adjusting the data polarization when the clock is circularly polarized. Changes in the polarization state produce a change ΔB in the background level, which can shift the zero-crossing point by as much as 700 fs.

BER versus the power measurements. To avoid this problem, we instead maintained a fixed input power and adjusted the optical signal-to-noise ratio (OSNR) by injecting a broadband amplified spontaneous emission prior to the clock recovery and receiver. Fig. 9(a) plots the measured Q-value as a function of the OSNR for a back-to-back transmission using both the recovered clock and the original clock. The Q-value was determined by measuring the BER as a function of the decision threshold, as depicted in Fig. 9(b). There is no significant difference between the two curves, which shows that there is no performance penalty associated with the clock recovery system.

IV. Polarization Dependence in Clock Recovery

As described in Section II, when the clock is circularly polarized, the amplitude of the cross correlation does not depend on the data polarization state. We exploited this polarization insensitivity in achieving the results shown in Figs. 7–9. Unfortunately, even with a circularly polarized clock signal, the background level B can vary with the data polarization, as described in (7). This variation ΔB is shown in Fig. 10, which plots the measured cross correlation between the clock and the data when the PLL is deactivated. The two curves in Fig. 10 show the maximum shift in the background level that can be obtained by adjusting the data polarization state while maintaining a circular state for the clock.

As shown in Fig. 10, after a fixed offset is subtracted, the cross-correlation signal exhibits a zero crossing for any input polarization state. This ensures that the clock recovery system can acquire and maintain lock regardless of the data polarization: a prediction that we have verified experimentally.

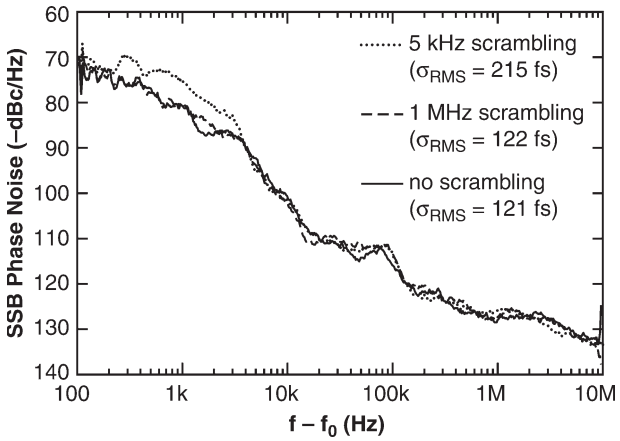

Fig. 11. Measured single-sideband phase noise of the recovered clock, when the data polarization state is scrambled at two different speeds. When the polarization fluctuations are within the PLL bandwidth, the timing jitter increases as a result of polarization-induced timing fluctuations.

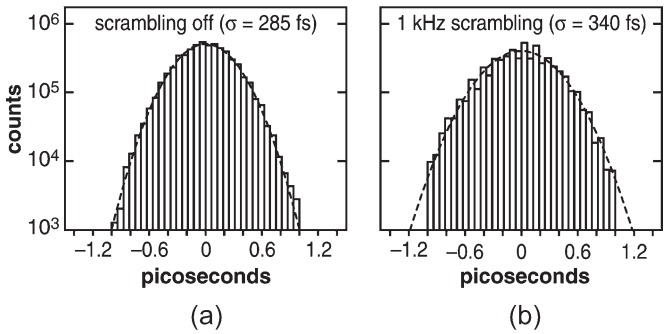

Fig. 12. Histograms showing the timing variations in the recovered clock, measured with a high-speed sampling oscilloscope. The RMS timing jitter is observed to increase when the polarization state is scrambled.

This condition will be maintained provided that the maximum change in the background level does not exceed the peak-to-peak amplitude of the cross-correlation signal, i.e., $\Delta B < C_0$.

The ratio $\Delta B/C_0$ can be estimated using (6)–(7). For simplicity, we assume that the clock and data are comprised of Gaussian pulses with pulsewidths of T and T' and that the pulses are sufficiently short that the cross-correlation function $C(\tau)$ goes almost to zero at the point of minimum overlap. Under this condition, we obtain

$$\frac{\Delta B}{C_0} = \frac{\langle p'^2(t)\rangle}{4\langle p(t)p'(t)\rangle} = \frac{1}{4}\sqrt{\frac{T^2+T'^2}{2T'^2}}\left(\frac{P'_{\rm avg}}{P_{\rm avg}}\right) \qquad (8)$$

where $P_{\rm avg}$ and $P'_{\rm avg}$ represent the time-averaged powers of the clock and data, respectively, and the data power is averaged over a random sequence of equally likely ones and zeros. Equation (8) holds for all data rates and also applies when the data rate is a multiple of the clock frequency.

Equation (8) reveals that once the data and clock pulsewidths are known, the ratio $\Delta B/C_0$ depends only on the ratio of the average powers. One can therefore minimize the sensitivity to polarization fluctuations by choosing the clock to be circularly polarized with the average power much larger than the data. Unfortunately, this choice also causes the signal amplitude C_0 to become much smaller than the total background level B, which degrades the OSNR in the avalanche photodiode. For the experiments reported here, we compromised by choosing the clock power to be twice as high as the data power.

As shown in Fig. 10, when the data polarization changes, the position of the zero crossing can vary by up to 700 fs, which produces a corresponding shift in the timing of the recovered clock. In order to study the effect of the polarization-induced timing fluctuations, we inserted a variable-speed polarization scrambler prior to the clock recovery system. Fig. 11 plots the measured phase-noise spectrum of the recovered clock for two different scrambling speeds. When the polarization is scrambled at 1 MHz, we see no significant increase in the phase noise of the recovered clock compared to the unscrambled system, because in this case, the speed of the PLL (5.5 kHz) is not fast enough to track the rapid changes caused by the polarization scrambling. However, when the polarization is scrambled at 1 kHz, the phase noise shows a marked increase at low frequencies, and the timing jitter increases from 121 to 215 fs as a result of low-frequency polarization fluctuations. Assuming that the polarization-induced fluctuations are uncorrelated with the intrinsic clock jitter, the timing fluctuations associated with polarization variations is 180 fs.

The effect of the polarization fluctuations can also be measured by observing the recovered clock signal on a high-speed sampling oscilloscope, using the original clock signal as a trigger. The histograms shown in Fig. 12 plot the statistical distribution in the timing of the recovered clock, accumulated over approximately 400 000 samples. We used a precision time-based system (Agilent 86107A) to reduce the effect of the intrinsic sampling jitter. The root-mean-square (rms) timing jitter increases from 285 to 340 fs when the polarization scrambling is enabled. These figures are considerably larger than those obtained from the phase-noise measurements, in part because of the large intrinsic jitter of the sampling oscilloscope, which was estimated to be 170 fs. Despite these limitations, the component of the timing jitter due to polarization fluctuations can be calculated by subtracting the variances, which gives 185 fs, in agreement with the independent phase-noise measurements.

As shown in (6), the background photocurrent and zero-crossing point depend only on the degree of ellipticity of the data polarization, which is described by the azimuthal angle θ ($\cos^2(\theta) = S'^2_3$) on the Poincaré sphere. If the cross correlation is approximated as a linear function of τ in the vicinity of the zero-crossing point, then (7) can be used to derive the following simple relationship between the zero-crossing time and the ellipticity:

$$\tau_{\rm z} = \tau_{\rm min} + \Delta\tau\cos^2(\theta) \qquad (9)$$

where $\Delta\tau$ is the maximum shift in the zero-crossing level. From the data plotted in Fig. 10, we infer that $\Delta\tau = 700$ fs.

Fig. 13(a) plots the measured distribution of the polarization states on the Poincaré sphere when the polarization is scrambled. Fig. 13(b) plots the predicted distribution of azimuthal angles θ for points that are uniformly distributed on the Poincaré

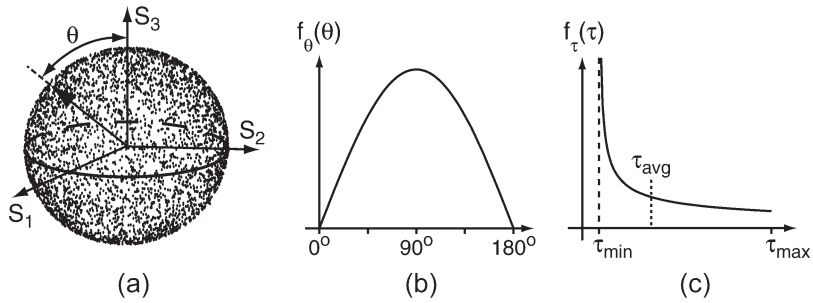

Fig. 13. (a) Sampled distribution of polarization states produced by the polarization scrambler, showing a uniform coverage of the Poincaré sphere. (b) Calculated probability distribution for the azimuthal angle θ for a point randomly located on the Poincaré sphere. (c) Probability distribution of zero-crossing time, which depends only on the azimuthal angle θ through (9).

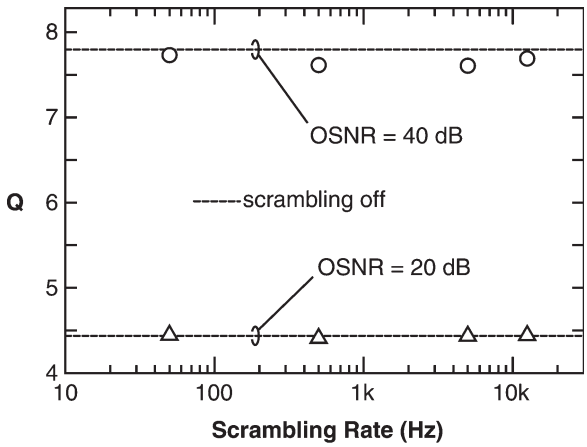

Fig. 14. Q as a function of the speed of polarization scrambling, measured at two representative OSNR levels. The dashed line indicates the value of Q obtained without scrambling.

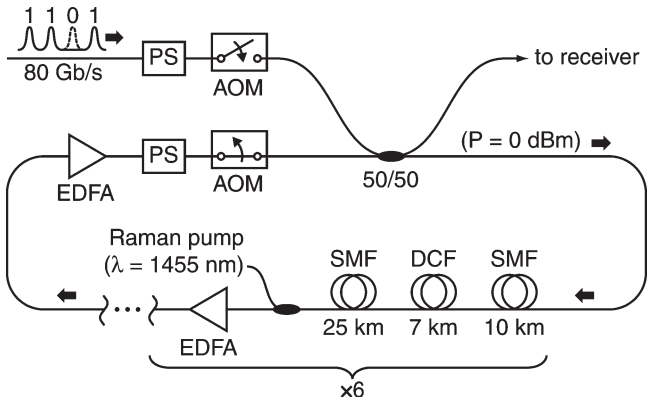

Fig. 15. Diagram of recirculating loop used to test the clock recovery system in a transmission environment.

sphere, and Fig. 13(c) plots the corresponding distribution of zero-crossing times, based on (9). Although the polarization states are uniformly distributed over the Poincaré sphere, the distribution of zero-crossing times is highly skewed toward the shorter times. By calculating the variance of this distribution, we predict that the RMS timing jitter associated with slow polarization variations will be

$$\sigma_{\mathrm{pol}} = 0.298\Delta\tau \simeq 210 \text{ fs}. \tag{10}$$

This result agrees approximately with the 180-fs figure inferred from experimental measurements. Furthermore, a careful examination of the histogram in Fig. 12(b) reveals a slight asymmetry when compared to the symmetric Gaussian curve indicated by the dashed line, which is explained by the skewed distribution described in Fig. 13(c).

In order to determine whether the polarization fluctuations lead to any real system impairment, we measured the BER as a function of the polarization-scrambling rate for two representative OSNR levels. The data points in Fig. 14 plot the measured Q-value for four different polarization-scrambling rates ranging from 50 Hz to 12 kHz, and the dashed lines indicate the value of Q obtained without the polarization scrambling. Although the Q-value depends on the OSNR, we observed no significant change in the BER or Q as a result of the polarization scrambling.

V. Transmission Experiments

The measurements described in the foregoing sections were all conducted with the transmitter and receiver connected back to back. In reality, the clock recovery is only required when the transmitter and receiver are physically separated. To test the clock recovery system in a transmission environment, we used the recirculating loop configuration shown in Fig. 15. The length of the loop is 210 km, which is divided into six identical dispersion maps. Each dispersion map is comprised of 10 km of conventional single-mode fiber (SMF) (Corning SMF-28, $D = 17$ ps/nm $\cdot$ km), 7 km of dispersion-compensating fiber (DCF), which is followed by an additional 25 km of SMF. The DCF was designed to compensate for both the dispersion and dispersion slope of the SMF, and the length of the DCF is not included in the propagation distances quoted here. A combination of the backward-pumped Raman amplification and conventional Erbium-doped fiber amplifiers (EDFAs) were used to compensate for fiber losses.

The signal emerging from the circulating loop consists of discontinuous packets of data that have each been circulating for increasing numbers of round trips. In order for the clock recovery system to operate properly in this configuration, it must quickly acquire lock at the beginning of each packet before the BER measurements can commence.

Fig. 16(a) plots the closed-loop step response of the clock recovery system, which was measured by observing how the error signal responds when a square-wave stimulus is artificially applied inside of the PLL. The dashed curve in Fig. 16(a)

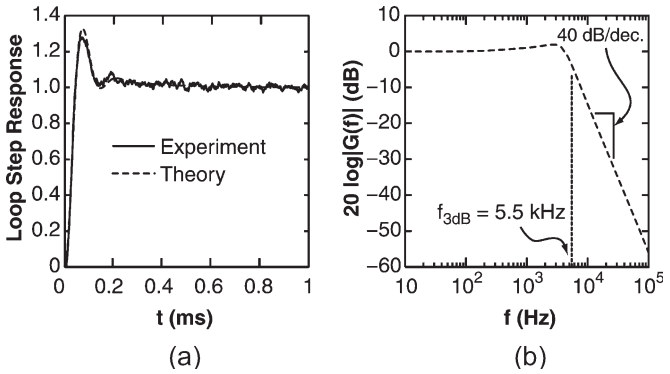

Fig. 16. (a) Measured and theoretically predicted step response of the PLL clock recovery system. The system exhibits a rise time below 0.20 ms. (b) Corresponding closed-loop spectral response of the PLL, showing a bandwidth of 5.5 kHz.

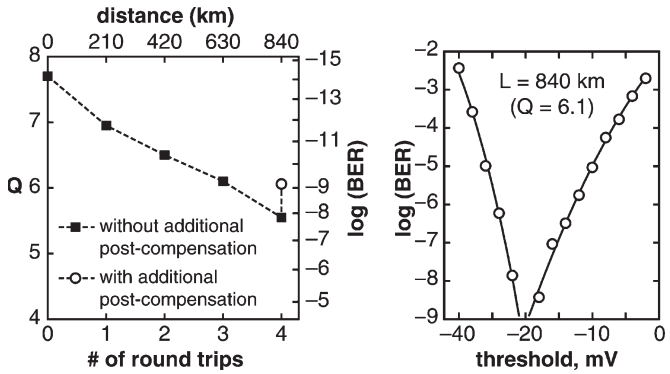

Fig. 17. (a) Measured Q-value versus the number of round trips (distance) in the circulating loop. Error-free ($Q > 6$) performance was achieved after four round trips by inserting an additional 100 m of fiber to compensate for residual dispersion in the loop. (b) BER versus threshold, measured after four round trips.

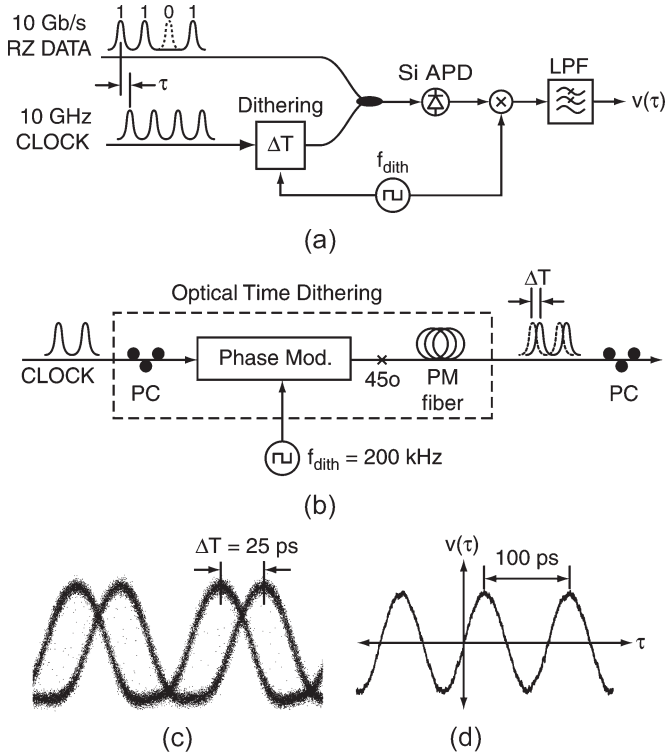

Fig. 18. (a) Diagram of the dithering clock recovery experiment. (b) Time dithering is accomplished by using an electrooptic phase modulator with the PM fiber. (c) Measured eye diagram of the dithered clock. The dither amplitude of 25 ps is determined by the length of the PM fiber. (d) Measured error signal always exhibits a zero crossing at $\tau = 0$.

plots the theoretically calculated step response, which shows excellent agreement with the measurements. Fig. 16(b) plots the corresponding spectrum of the closed loop transfer function, showing the bandwidth of 5.5 kHz. The rise time for the PLL is approximately 0.15 ms, whereas the packet length for the 250-km circulating loop is 1.25 ms. Therefore, the clock-recovery system can stabilize within the first 20% of each packet, still allowing an ample of time to conduct the BER measurements before the next packet arrives.

Using this system, we successfully demonstrated error-free 80-Gb/s transmission over 1000 km (or 840 km, not counting the DCF modules). Fig. 17 plots the measured BER versus the threshold level after 1000 km. The details of these transmission experiments are described elsewhere [20], but we emphasize here that because of the unique clock recovery system, we were able to achieve these results without using any polarization control in the transmitter or receiver.

VI. Dithering Phase Detection

One disadvantage of the clock recovery scheme described here is that the background level depends on the input data power and polarization state. As described in Section IV, in such a system, the ratio between the average powers of the clock and the data signals should be selected carefully in order to minimize the polarization sensitivity. Even when selected properly, variations in the input power levels or ambient light levels in the laboratory can change the background photocurrent, which can cause a timing jitter or even synchronization loss.

One solution to this problem is to generate the bipolar error signal using balanced detectors [9], [13], [21]. This would require two matched silicon detectors with identical avalanche gain, which adds to the cost and complexity of the system. Another approach that can track the peak of the cross correlation using only one detector is to dither the timing of the clock signal by modulating the phase of the voltage-controlled oscillator [15], [22]. When the resulting cross-correlation signal is mixed with the dithering signal and lowpass filtered, it produces a bipolar error signal that approximates the slope of the original cross-correlation function. The only disadvantage of this technique is that the recovered optical and electrical clocks are dithered and exhibiting spectral sidebands at the dither frequency. Because it is hard to remove these components from the final clock signal, the recovered clock may be unsuitable for later use in the optical regeneration or transmission.

To overcome those issues, we have developed an optical time-dithering system depicted in Fig. 18(a). We have tested the optical dithering system at 10 Gb/s as a proof of concept, and we expect the system to operate at higher speeds.

The optical dithering system is comprised of an electrooptic phase modulator followed by a length of birefringent polarization-maintaining (PM) fiber, as depicted in Fig. 18(b). The clock polarization is adjusted so that the clock signal

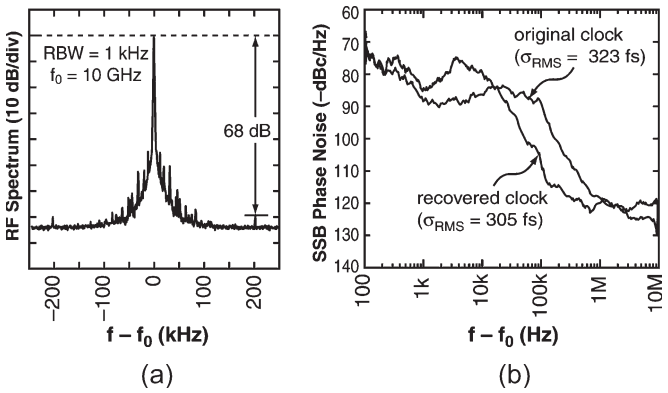

Fig. 19. (a) RF spectrum and (b) single-sideband phase noise of the recovered 10-GHz electrical clock. The dither tones at ± 200 kHz is suppressed by 68 dB.

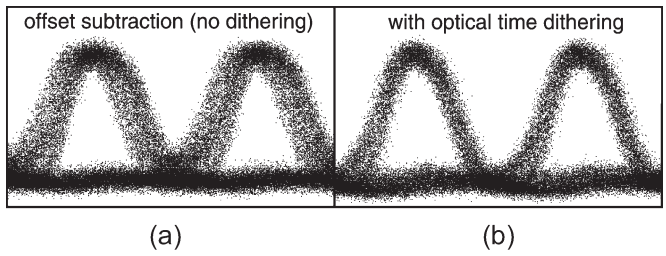

Fig. 20. Eye diagram of the received 10-Gb/s data, measured while the polarization state is varied. (a) Undithered system exhibits a significant polarization-dependent timing, as described in Section IV. (b) Dithering clock recovery instead locks to the peak of the cross-correlation signal, which reduces the polarization dependence.

entering the phase modulator is linearly polarized at 45° to the z-axis of the modulator. The phase modulator is driven with a square wave at frequency $f_{\rm dith} = 200$ kHz. When the amplitude of the square wave is adjusted properly, the signal emerging from the modulator is periodically switched between two orthogonal polarization states at $\pm 45°$. The axes of the PM fiber are also oriented at $\pm 45°$ with respect to the modulator, so that the signal enters into the fast and slow axis of the fiber, depending on the applied voltage. The amplitude of the timing dither is then entirely determined by the length and birefringence of the PM fiber. The advantage of this scheme over other dithering approaches is that it allows access to the undithered optical and electrical clock.

Fig. 18(c) shows the dithered optical clock measured on a sampling oscilloscope in eye diagram mode. The amount of timing dither is 25 ps, which was achieved by using 18 m of the PM fiber. The dithered clock signal alternates between two orthogonal polarization states, and by using a manual polarization controller, it is possible to convert these two states to the right- and left-hand circular polarizations, which are optimal for polarization-insensitive performance.

After the clock and data signals are combined and focused onto the silicon avalanche photodiode, the resulting photocurrent is mixed with a reference dither signal and lowpass filtered. Fig. 18(d) plots the resulting error signal $v(\tau)$, which approximates the derivative of the original cross-correlation signal $C(\tau)$. Unlike the original cross-correlation signal, which exhibits a nonzero background, the dithered phase-detection circuit always produces a bipolar error signal $v(\tau)$, which has a zero crossing when $\tau = 0$, as shown in Fig. 18(d).

Fig. 19(a) plots the electrical spectrum of the 10-GHz recovered clock obtained with the dithering PLL. The dithering tones at ± 200 kHz offset frequency can be seen on the spectrum, but they are suppressed by 68 dB compared to the carrier. We estimate that these sidebands increase the timing jitter by only 9 fs. When we instead produced the same 25-ps timing dither by electrical phase modulation, we observed that the sidebands increase to only 8 dB below the carrier.

Fig. 19(b) plots the single-sideband phase-noise of the recovered clock and original transmitter clock. The integrated phase noise from 100 Hz to 1 MHz was 305 fs for the recovered clock, compared to 323 fs for the original clock.

One of the advantages of this system compared to the system that is based on the offset subtraction (explained in Section III), is a lower polarization sensitivity. As discussed in Section IV, changes in the data polarization can cause a shift in the background level, which in the conventional system induces a corresponding shift in the timing of the recovered clock. The dithering system by contrast does not require the subtraction of an offset signal, and it is therefore expected to perform much better in the presence of polarization or power fluctuations.

This effect is clearly illustrated in Fig. 20, which plots the eye diagram of the received data when the recovered clock signal is used as a trigger. In both cases, the polarization state of the data was randomly varied during the measurement. When the offset-subtraction method is used, we see a significant broadening of the eye as a result of polarization-induced timing fluctuations. By contrast, when the new dithering phase detection is used, the eye diagram remains stable even when the polarization state changes.

The dithering system brings a similar improvement to the dynamic range of the clock recovery system. To quantify this improvement, we varied the power of the data signal while keeping the clock average power fixed at 5 mW. The ratio of the data to the clock power was varied from -8 to $+2$ dB, and the system was able to acquire and maintain lock at all of these power levels. For comparison, the conventional subtraction technique requires adjustment of the offset value whenever the data power changes.

In the prototype 10-Gb/s system described in this section, the data was produced by externally modulating a tunable CW laser. This allowed us to investigate the wavelength dependence of the clock recovery system—something that is difficult to explore with mode-locked lasers. For silicon, TPA can theoretically be observed for wavelengths from 1100–2200 nm, a range that encompasses the entire spectrum that is presently used in the fiber-optic communication. We successfully tested the clock recovery system at wavelengths from 1534 to 1568 nm, which is a range limited only by the bandwidth of our EDFAs, and found that it functioned properly at all wavelengths tested.

VII. Conclusion

In conclusion, TPA in a simple inexpensive silicon photodiode can be used as an ultrafast tool in high-speed optical-communication networks. Cross-correlation measurement

using this nonlinear detection process was discussed in terms of polarization and power dependence. The concept of optical clock recovery using TPA was experimentally proved in an 80-Gb/s transmission experiment, providing a low timing jitter, low polarization dependence, and broad optical bandwidth. The use of the system in a 210-km long recirculating loop was successfully tested, and 840-km transmission with an error-free operation was achieved. Removing the offset variation from the error signal was concluded to be a major improvement in the system, reducing its polarization dependence, increasing its power dynamic range, and increasing its optical bandwidth. A novel optical dithering system was demonstrated as a tool for realizing the offset-free scheme. Preliminary experiments on the offset-free system operating at 10 Gb/s show at least 10 dB of power dynamic range, polarization independence, and at least 35-nm optical bandwidth, which is mainly limited by the EDFA bandwidth.

REFERENCES

[1] Y. Li, C. Kim, G. Li, Y. Kaneko, R. L. Jungerman, and O. Buccafusca, "Wavelength and polarization insensitive all-optical clock recovery from 96-Gb/s data by using a two-section gain-coupled DFB laser," *IEEE Photon. Technol. Lett.*, vol. 15, no. 4, pp. 590–592, Apr. 2003.

[2] Y. Yang, Y. J. Wen, A. Nirmalathas, H. F. Liu, and D. Novak, "Optical clock recovery at line rates via injection locking of a long cavity Fabry–Pérot lase diode," *IEEE Photon. Technol. Lett.*, vol. 16, no. 6, pp. 1561–1563, Jun. 2004.

[3] T. Ohno, K. Sato, R. Iga, Y. Kondo, T. Ito, T. Furuta, K. Toshino, and H. Ito, "Recovery of 160 GHz optical clock from 160 Gb/s data stream using modelocked laser diode," *Electron. Lett.*, vol. 40, no. 4, pp. 265–267, 2004.

[4] Z. Hu, H.-F. Chou, K. Nishimura, M. Usami, J. E. Bowers, and D. J. Blumenthal, "Optical clock recovery circuits using travelling-wave electroabsorption modulator-based ring oscillator for 3R regeneration," *IEEE J. Sel. Topics Quantum Electron.*, vol. 11, no. 2, pp. 329–337, Mar./Apr. 2005.

[5] J. Lasri, P. Devgan, R. Tang, and P. Kumar, "Ultralow timing jitter 40 Gb/s clock recovery using a self-staring optoelectronic oscillator," *IEEE Photon. Technol. Lett.*, vol. 16, no. 1, pp. 263–265, Jan. 2004.

[6] H. Tsuchida and M. Suzuki, "40 Gb/s optical clock recovery using an injection-locked optoelectronic oscillator," *IEEE Photon. Technol. Lett.*, vol. 17, no. 1, pp. 211–213, Jan. 2005.

[7] T. Saito, Y. Yano, and N. Henmi, "Optical TDM 20 Gb/s–105 km transmission employing newly proposed optical PLL timing extraction," *IEEE Photon. Technol. Lett.*, vol. 6, no. 4, pp. 555–557, Apr. 1994.

[8] O. Kamatani and S. Kawanishi, "Ultra-high speed clock recovery with phase lock loop based on four-wave mixing in a travelling-wave laser diode amplifier," *J. Lightw. Technol.*, vol. 14, no. 8, pp. 1757–1767, Aug. 1996.

[9] E. Awad, P. S. Cho, N. Moulton, and J. Goldhar, "Subharmonic optical clock recovery from 160 Gb/s using time-dependent loss saturation inside a single electroabsorption modulator," *IEEE Photon. Technol. Lett.*, vol. 15, no. 12, pp. 1764–1766, Dec. 2003.

[10] T. Yamamoto, L. K. Oxenlowe, C. Schmidt, C. Schubert, E. Hilliger, U. Feiste, J. Berger, R. Ludwig, and H. G. Weber, "Clock recovery from 160 Gb/s data signals using phase-locked loop with interferometric optical switch based on semiconductor optical amplifier," *Electron. Lett.*, vol. 37, no. 8, pp. 509–510, 2001.

[11] D. T. K. Tong, B. Mikkelsen, G. Raybon, T. N. Nielsen, K. F. Dreyer, and J. E. Johnson, "Optoelectronic phase-locked loop with balanced photodetection for clock recovery in high-speed optical time-division-multiplexed systems," *IEEE Photon. Technol. Lett.*, vol. 12, no. 8, pp. 1064–1066, Aug. 2000.

[12] S. Takasaka, Y. Ozeki, K. Igarashi, and S. Namiki, "Optical phase-locking of 160 GHz optical beat to 40 GHz optical pulse train using a three-electrode DFB-LD and a Si avalanche photodiode," in *Proc. Eur. Conf. Opt. Commun.*, 2005, vol. 4, pp. 799–800.

[13] C. Boerner, C. Schubert, C. Schmidt, E. Hilliger, V. Marembert, J. Berger, S. Ferber, E. Diertrich, R. Ludwig, B. Schmauss, and H. G. Weber, "160 Gb/s clock recovery with electro-optical PLL using bidirectionally operated electroabsorption modulator as phase comparator," *Electron. Lett.*, vol. 39, no. 14, pp. 1071–1073, 2003.

[14] Y. J. Wen, C.-J. Chae, and H. F. Liu, "Time-domain polarization interleaving of signal to allow polarization-insensitive all-optical clock recovery," *IEEE Photon. Technol. Lett.*, vol. 17, no. 6, pp. 1304–1306, Jun. 2005.

[15] T. Sakamoto, K. Seo, K. Taira, N. S. Moon, and K. Kikuchi, "Polarization-insensitive all-optical time-division demultiplexing using a fiber four-wave mixer with a peak-holding optical phase-locked loop," *IEEE Photon. Technol. Lett.*, vol. 16, no. 2, pp. 563–565, Feb. 2004.

[16] T. Hasegawa, K. Inoue, and K. Oda, "Polarization independent frequency conversion by fiber four-wave mixing with a polarization diversity technique," *IEEE Photon. Technol. Lett.*, vol. 5, no. 8, pp. 947–949, Aug. 1993.

[17] R. Salem and T. E. Murphy, "Polarization-insensitive cross-correlation using two-photon absorption in a silicon photodiode," *Optics Lett.*, vol. 29, no. 13, pp. 1524–1526, Jul. 2004.

[18] M. E. Marhic, K. K. Y. Wong, and L. G. Kazovsky, "Fibre optical parametric amplifiers with circularly-polarised pumps," *Electron. Lett.*, vol. 39, no. 4, pp. 350–351, Feb. 2003.

[19] R. Salem, G. E. Tudury, T. U. Horton, G. M. Carter, and T. E. Murphy, "Polarization-insensitive optical clock recovery at 80 Gb/s using a silicon photodiode," *IEEE Photon. Technol. Lett.*, vol. 17, no. 9, pp. 1968–1970, Sep. 2005.

[20] G. E. Tudury, R. Salem, G. M. Carter, and T. E. Murphy, "Transmission of 80 Gb/s over 840 km in standard fibre without polarisation control," *Electron. Lett.*, vol. 41, no. 25, pp. 1394–1396, Dec. 2005.

[21] T. F. Carruthers and J. W. Lou, "80 to 10 Gb/s clock recovery using phase detection with Mach–Zehnder modulator," *Electron. Lett.*, vol. 37, no. 14, pp. 906–907, Jul. 2001.

[22] I. D. Phillips, A. Gloag, P. N. Kean, N. J. Doran, I. Bennion, and A. D. Ellis, "Simultaneous demultiplexing, data recognition, and clock recovery with a single semiconductor optical amplifier-based nonlinear-optical loop mirror," *Optics Lett.*, vol. 22, no. 17, pp. 1326–1328, 1997.

Reza Salem (S'00) was born in Tehran, Iran, in July 1979. He received the B.S. degree in electrical engineering from Sharif University of Technology, Tehran, Iran, in 2001. He is currently working toward the Ph.D. degree with the Department of Electrical and Computer Engineering, University of Maryland, College Park.

His research interests are in the area of optical communication systems. He is currently investigating applications of two-photon absorption in high-speed optical communication systems.

Amir Ali Ahmadi is an undergraduate student with University of Maryland, College Park, where he is studying mathematics and electrical engineering. He will begin graduate study in electrical engineering at the Massachusetts Institute of Technology (MIT), Cambridge, in Fall 2006.

Gaston E. Tudury was born in Buenos Aires, Argentina. He received the Licenciado en Cs. F'isicas degree in physics from the Universidad de Buenos Aires and the Ph.D. degree in physics, performing research on spectroscopic studies of quantum structures using ultrafast laser systems, from Universidade Estadual de Campinas, Campinas, Sao Paulo, Brazil, in 2001.

In October 2001, he was a Research Associate with University of Maryland, Baltimore County. He later performed research in fiber-optic communications with the Laboratory for Physical Sciences, University of Maryland, College Park.

Gary M. Carter (M'82–SM'85) received the Ph.D. degree in physics from the Massachusetts Institute of Technology (MIT), Cambridge, in the area of atomic and molecular beam scattering.

Subsequently, he carried out research in the area of infrared radar and infrared nonlinear optics with MIT's Lincoln Laboratory, Lexington. Following this, he investigated ultrafast processes in polymers with GTE's corporate research laboratories and coherent optical communications with MIT's Lincoln Laboratory. He was appointed to the Electrical Engineering Faculty with the University of Maryland, Baltimore County, in 1988, and since then, he has carried out research in modelocked lasers, biosensors, and high-speed optical communications.

Thomas E. Murphy (M'94) studied physics and electrical engineering and received the joint B.A./B.S.E.E. degrees from Rice University, Houston, TX, in 1994. In 1994, he joined the NanoStructures Laboratory, Massachusetts Institute of Technology (MIT), Cambridge, where he pursued research in integrated optics and nanotechnology. He received the M.S. and Ph.D. degrees, both in electrical engineering, from MIT in 1997 and 2000, respectively.

In 2000, he joined the MIT Lincoln Laboratory, Lexington, as a Staff Member in the Optical Communications Technology Group, where he studied and developed ultrafast optical communications systems. In August 2002, he joined the faculty of the University of Maryland, College Park, as an Assistant Professor with the Department of Electrical and Computer Engineering. His research interests include optical communications, short-pulse phenomena, numerical simulation, optical pulse propagation, nanotechnology, and integrated photonics.

Dr. Murphy is a member of the Optical Society of America (OSA) and a recipient of the NSF CAREER Award.